Biomechanical evaluation of a novel anatomical plate for oblique lumbar interbody fusion compared with various fixations: a finite element analysis

Weibo Huang[#], Ye Tian[#], Xiaosheng Ma, Feizhou Lv, Hongli Wang[*], Jianyuan Jiang[*]

Department of Orthopedics, Huashan Hospital, Fudan University, Shanghai, China

Contributions: (I) Conception and design: H Wang, W Huang; (II) Administrative support: J Jiang, F Lv; (III) Provision of study materials or patients: X Ma; (IV) Collection and assembly of data: Y Tian; (V) Data analysis and interpretation: W Huang, Y Tian; (VI) Manuscript writing: All authors; (VII) Final approval of manuscript: All authors.

[#]These authors contributed equally to this work and should be considered as co-first authors.

*These authors contributed equally to this work and should be considered as co-corresponding authors.

Correspondence to: Jianyuan Jiang; Hongli Wang. Department of Orthopedics, Huashan Hospital, Fudan University, 12 Mid-Wulumuqi Road, Shanghai 200040, China. Email: 13301050222@fudan.edu.cn; wanghongli0212@163.com.

Background: To build a model of an anatomical plate for oblique lumbar interbody fusion (OLIF) surgery based on previous anatomical parameters and verify the biomechanical effect with finite element analysis.

Methods: The anatomical plate model was built with AutoCAD and Solidworks. Finite element models of the L2–3 and L4–5 segments were established with computed tomography images from a 46-year-old asymptomatic male individual. Six fixation technique models were created: (I) stand-alone (SA); (II) bilateral pedicle screws (BPS); (III) lateral rod-screw (LRS); (IV) lateral rod-screw plus facet screw (LRSFS); (V) two-screw lateral plate (TSLP); (VI) anatomical plate. The range of motion (ROM), the cage stress, and the instrument stress were calculated under different motion states.

Results: In the L2–3 and L4–5 segment models, except for a slightly higher maximum cage stress in the extension state of the TSLP model and the right bending and rotation states of the BPS model, the maximum cage stress in each model was smaller than that of the SA model. In the L2–3 and L4–5 segments, each internal fixation limited the ROM in each motion state. The anatomical plate was more effective in reducing the maximum cage stress and vertebral ROM than the two-screw plate. Three-dimensional finite element analysis did not find a higher risk of construct failure for the anatomical plate model compared with the BPS internal fixation model.

Conclusions: Anatomical plates can be considered as supplementary fixations using a single incision and position to improve the stability and rigidity of the construction and reduce the risk of complications.

Keywords: Anatomical oblique lateral plates; oblique lumbar interbody fusion (OLIF); biomechanical evaluation; finite element study

Submitted Jun 20, 2022. Accepted for publication Jul 27, 2022.
doi: 10.21037/atm-22-3456
View this article at: https://dx.doi.org/10.21037/atm-22-3456

Introduction

Oblique lumbar interbody fusion (OLIF) reduces the damage to posterior anatomical structures, such as ligaments and paravertebral muscles, involved in posterior or transforaminal lumbar interbody fusion. Therefore, OLIF has been considered capable of preserving the biomechanical stability of the posterior lumbar column and reducing the risk of related complications caused by intraoperative nerve root traction (1,2).

Currently, clinicians mainly adopt two surgical

Table 1 Mechanical properties of the involved components

Component	Young's modulus (MPa)	Poisson's ratio
Cortical bone	12,000	0.30
Cancellous bone	100	0.30
Facet joint cartilage	50	0.30
Endplate	1,000	0.40
Nucleus	1	0.49
Annulus fibrosus	4.2	0.45
Anterior longitudinal ligament	20	0.30
Posterior longitudinal ligament	20	0.30
Transverse ligament	59	0.30
Interspinous ligament	12	0.30
Ligamentum flavum	19.5	0.30
Supraspinous ligament	15	0.30
PEEK	3,000	0.30
Bone graft	450	0.29
Titanium alloy	110,000	0.30

PEEK, poly-ether-ether-ketone.

techniques: the first simply implants the cage into the intervertebral space [stand-alone (SA) technology], and the other inserts a percutaneous pedicle screw after placing the cage. However, current internal fixation techniques still have some deficiencies that require improvement. For instance, some studies have reported that SA technology is associated with insufficient immediate stability, a longer bed-rest time, and a higher risk of cage subsidence or pseudoarthrosis (3,4). The bilateral percutaneous pedicle screw offers stronger fixation, but the patient needs to be repositioned in the prone position under anesthesia, resulting in a longer operative time. An additional small incision is also required, and the technique results in more radiation exposure for both the patient and surgeon (5,6).

Several previous studies have reported the use of plate and screw fixation systems for OLIF and have demonstrated the biomechanical efficiency of the system (7,8). However, these studies have two noteworthy limitations and could be further improved. First, previous studies have not provided clear references for the anatomical parameters that the length, width, or curvature of the plates depend on. Second, the biomechanical tests mainly focus on a single lumbar segment. Therefore, the use of plates might cause injury to significant structures, such as the abdominal aorta and segmental arteries, and there is a lack of solid proof that the same size plates can be used for different segments (9,10).

To address these issues, the authors completed a series of anatomical studies to acquire the anatomical parameters associated with the plate design for OLIF (11,12). Based on these parameters, we attempted to develop novel and safe lateral plates with an anatomical design. The current study aimed to introduce the initial design and verify its biomechanical performance by comparison with various internal fixations, using finite element analysis. We present the following article in accordance with the MDAR reporting checklist (available at https://atm.amegroups.com/article/view/10.21037/atm-22-3456/rc).

Methods

Establishment of the lumbar spine model

The models used in the study were based on the computed tomography images from a 46-year-old male from the Department of Radiology at our hospital. The included subject had no medical history of lumbar degenerative diseases, infections, tumors, or deformities. The study was conducted in accordance with the Declaration of Helsinki (as revised in 2013). This study was approved by the institutional review board of Huashan Hospital, Fudan University (No. KY-2020-052). All participating patients signed informed consent to participate in this study, and any information or identification of the patients have been concealed. The L2 to L3 and L4 to L5 images were exported in a Digital Imaging and Communications in Medicine format and were then imported into Mimics Research 19.0 (Materialise NV, Leuven, Belgium) software to generate three-dimensional models. The polish was completed with Geomagic Studio 2013 (3D Systems, Inc., Rock Hill, South Carolina, USA). The 'Construct Patches' and 'Grid and Fit Surfaces' tools were used during the procedure, and the modified models were then exported in an STL format. The STL files were subsequently imported into SolidWorks 2017 computer-aided design software (Dassault Systèmes SolidWorks Corporation, Waltham, Massachusetts, USA). The involved elements were created, including cortical bone, cancellous bone, endplate, annulus fibrosus, nucleus pulposus, articular cartilage, and ligament. Then, the biomechanical properties of the different elements were set, and the elements were meshed based on previous research using ANSYS 17.0 software (ANSYS, Ltd., Canonsburg, Pennsylvania, USA) (5,13). The detailed biomechanical parameters are listed in *Table 1*. The meshed models were analyzed by ANSYS 17.0. Finally, two lumbar spine models, L2–3 and L4–5, were successfully established.

Boundary and loading conditions

The static biomechanical analysis was implemented by ANSYS 17.0. The boundary and loading conditions were set according to previous studies (5,13-15). The spring element was used to simulate the anterior longitudinal ligament, posterior longitudinal ligament, ligamentum flavum, intertransverse ligament, interspinous ligament, supraspinous ligament, and joint capsule structures. The relevant parameters were set by referring to the previous literature, and the stiffness was 8.7, 5.8, 15.4, 0.2, 10.9, 2.4, and 15.8 N/mm, respectively (5,13). The contact type between the facet joints, screws, and plates was set as ‘frictional’, and the friction coefficient was 0.2. Other contact types were set as the binding mode “bone”.

A combined follower load of 380 N was applied on the superior surface of the L2, and 7.5 N.m bending moments of flexion, extension, left/right bending, and left/right rotation were applied to simulate the physiological movements of the lumbar segments (10,16). The L4–L5 model was established similarly with a follower load of 400 N and 7.5 N.m bending moments. Subsequently, the range of motion (ROM) of the above models was recorded and compared with previous studies for validation of the model (17).

Surgical simulation

To simulate the OLIF procedure, the nucleus and part of the annulus fibrosus of the intervened intervertebral disc as well as adjacent endplates were removed. The cage was placed in the middle of the intervertebral space. A total of six internal fixation techniques were established based on the abovementioned L2–3 or L4–5 models as follows (*Figure 1*): (I) SA: a cage (40×18×12 mm^3) was implanted without other supplementary internal fixations; (II) bilateral pedicle screw (BPS): a cage (40×18×12 mm^3) was implanted with BPSs (length: 45 mm, outer diameters: 5.5 mm); (III) lateral rod-screw (LRS): after the cage had been located, two screws (length: 45 mm, outer diameters: 6.5 mm) were bicortically fixed on the vertebrae with a rod connection (length: 40 mm, diameters: 5 mm); (IV) lateral rod-screw plus facet screw (LRSFS): the lateral rod and screws were implanted as described above. An additional contralateral translaminar facet screw (outer diameters: 3.5 mm) was inserted from the contralateral aspect of the spinous process and then crossed the center of the facet joints and reached the base of the transverse process of the inferior vertebra; (V) two-screw lateral plate (TSLP): a cage (40×18×12 mm^3) was implanted with a conventional lateral plate (28×10×6.5 mm^3) fixed with two screws (length: 25 mm, outer diameters: 5.5 mm); (VI) anatomical lateral plate (ALP): according to previous research and our anatomical studies, we designed two ALPs for OLIF at L2–3 (length: 27 mm, width: 15 mm, height: 6 mm) and L4–5 (length: 35 mm, width: 12 mm, height: 6 mm) (*Figure 2*). The length of the plates depended on the distances between the adjacent lumbar segmental arteries to avoid arterial injury (11). The width was limited according to the surgical corridor (see Table S1). The sagittal arc was 6° for the L2–3 plate and 15° for the L4–5 plate (18). A coronal curvature of 0.6 cm^{-1} was acquired based on our previous study (12). There were six screws in the plates (3 screw holes in each side along the intervertebral discs). Two cancellous bone screws were inserted into the two central holes towards the center of the vertebrae, and four cortical screws were implanted from the surrounding holes, which were fixed bicortically on the vertebral endplates.

Statistical analysis

The calculation was performed after successfully building the models under the settled boundary and loading conditions. Using ANSYS 17.0 software analysis, the ROMs of the L2–3 and L4–5 segments of each internal fixation model were recorded under six physiological motion states. Additionally, the maximum Von-Mises stress of the plates, screws, and cages was recorded to evaluate the risk of construct failure and cage subsidence. For statistical analysis, the calculation was replicated for the mesh convergence test to decrease potential errors caused by the mesh size. With altered mesh size in a three-time technical replication, results that showed an almost stable solution with a variability of less than 5% were recognized as acceptable and recorded in this study. Data with abnormal stress concentration was excluded from the study. Descriptive statistics were used to present the trend acquired from the comparison and to provide direct diagrams for analysis. The datasets generated and analyzed during the current study are not publicly available due to their original design and individual privacy but are available from the corresponding author on reasonable request.

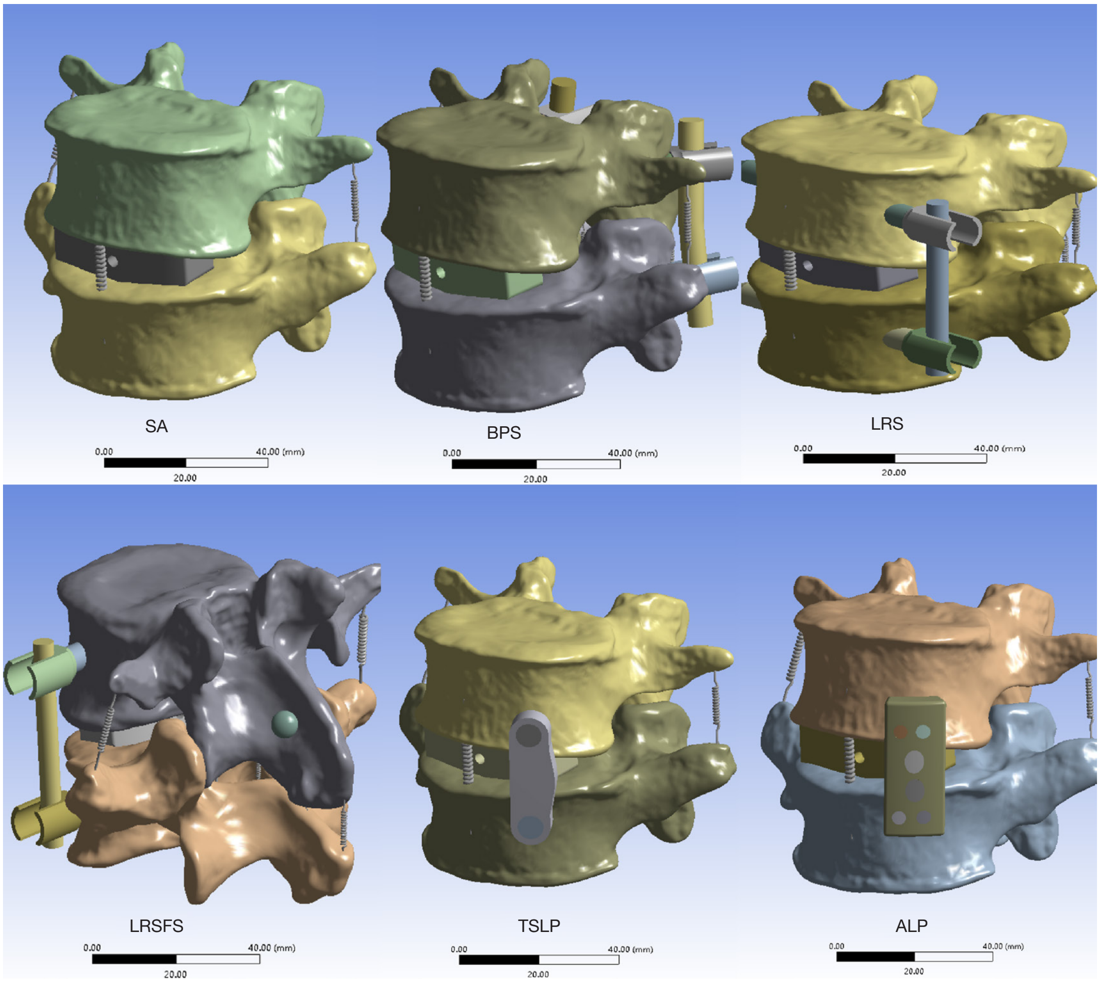

Figure 1 The construction of the OLIF models with various supplementary fixations. A total of six OLIF models with different internal fixations were constructed. SA, stand-alone; BPS, bilateral pedicle screw; LRS, lateral rod-screw; LRSFS, lateral rod-screw plus facet screw; TSLP, two-screw lateral plate; ALP, anatomical lateral plate; OLIF, oblique lumbar interbody fusion.

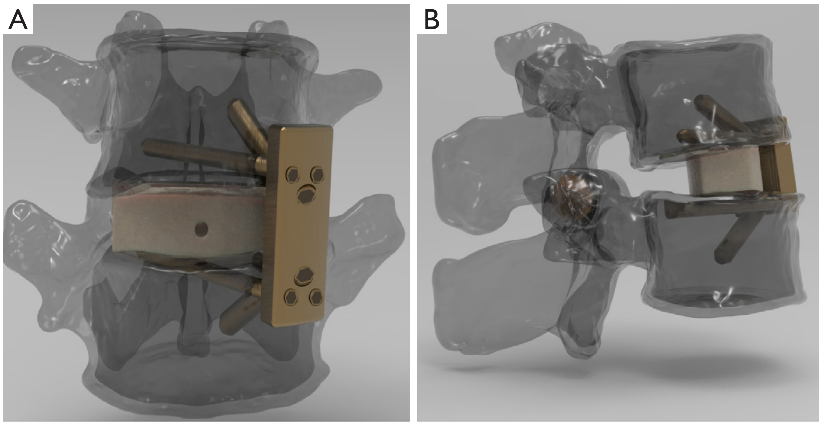

Figure 2 The installation technique of the anatomical plates. The design of the plates and screws and the location where the screws were inserted are shown in the figure.

Table 2 The range of motion of the L2–3 and L4–5 segments (°)

Model	Flexion	Extension	Left bending	Right bending	Left rotation	Right rotation
L2–3	6.1	3.8	7.2	6.2	2.8	2.3
L4–5	9.4	5.9	5.5	5.4	2.3	2.2

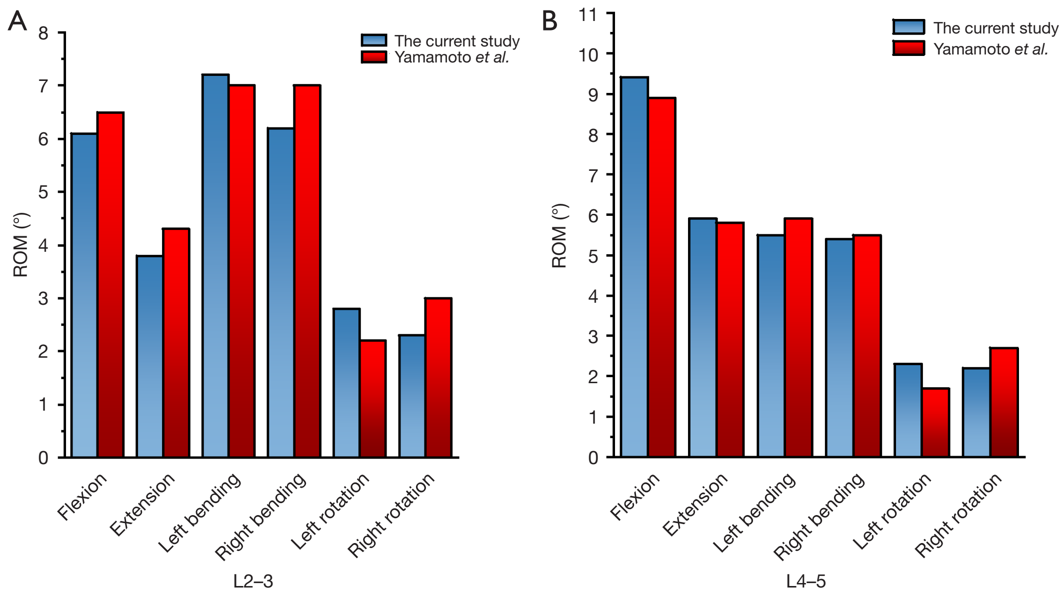

Figure 3 Validation of the constructed lumbar spine models. The ROMs of the lumbar spine models constructed in the current study compared with previous studies. The ROMs of the present model are in accordance with the results published previously. (A) The validation of the L2–3 model. (B) The validation of the L4–5 model. ROM, range of motion.

Results

Model validation

The ROMs of the L2–3 model under the flexion, extension, left bending, right bending, left rotation, and right rotation states were 6.1°, 3.8°, 7.2°, 6.2°, 2.8°, and 2.3°, respectively. For the L4–5 model, the ROMs were 9.4°, 5.9°, 5.5°, 5.4°, 2.3°, and 2.2° under the six motion states, respectively (*Table 2*). As shown in *Figure 3*, the ROMs of the present model were in accordance with the results published previously (5,17).

ROM

The ROMs of the L2–3 and L4–5 models with different fixation techniques are shown in *Table 3* and *Figure 4*. The SA fixation in both models showed the largest ROMs in all motion states, while the BPS and LRSFS constructs had the least ROMs. The use of LRS reduced the ROMs of left bending and right bending at L2–3 and L4-5. When the SA models were excluded, the LRS construct performed worst in reducing the ROMs of the flexion and extension states. The anatomical plates showed fair construct stability in both the L2–3 and L4–5 models. Specifically, the ALP model had a more satisfactory effect on reducing the ROMs in all motion states than the SA model. Moreover, the ALP models performed better than the conventional lateral plate in reducing the ROMs under all six motion states. Additionally, the ROMs of ALP models varied in different motion states. It could be noted that the ROMs in flexion/extension were largest while the ROMs in lateral/right rotation were smallest.

Loading of the cage

The maximum stress of the cages in the L2–3 model with various fixations is shown in *Table 4* and *Figure 5*. In

Table 3 The range of motion of the L2–3 and L4–5 segments in models with various fixations (°)

Model	Flexion	Extension	Left bending	Right bending	Left rotation	Right rotation
L2–3						
SA	1.62	2.00	0.72	0.59	0.16	0.17
BPS	0.53	0.35	0.39	0.36	0.09	0.12
LRS	1.51	1.73	0.33	0.52	0.12	0.12
LRSFS	0.54	0.39	0.31	0.35	0.10	0.12
TSLP	1.17	1.65	0.51	0.49	0.15	0.15
ALP	0.91	1.40	0.44	0.47	0.14	0.15
L4–5						
SA	1.93	2.48	0.52	0.35	0.14	0.15
BPS	0.52	0.42	0.34	0.29	0.13	0.12
LRS	1.70	2.11	0.27	0.31	0.13	0.13
LRSFS	0.58	0.45	0.27	0.32	0.12	0.11
TSLP	1.18	1.89	0.41	0.33	0.11	0.10
ALP	0.81	1.44	0.34	0.32	0.10	0.10

SA, stand-alone; BPS, bilateral pedicle screw; LRS, lateral rod-screw; LRSFS, lateral rod-screw plus facet screw; TSLP, two-screw lateral plate; ALP, anatomical lateral plate.

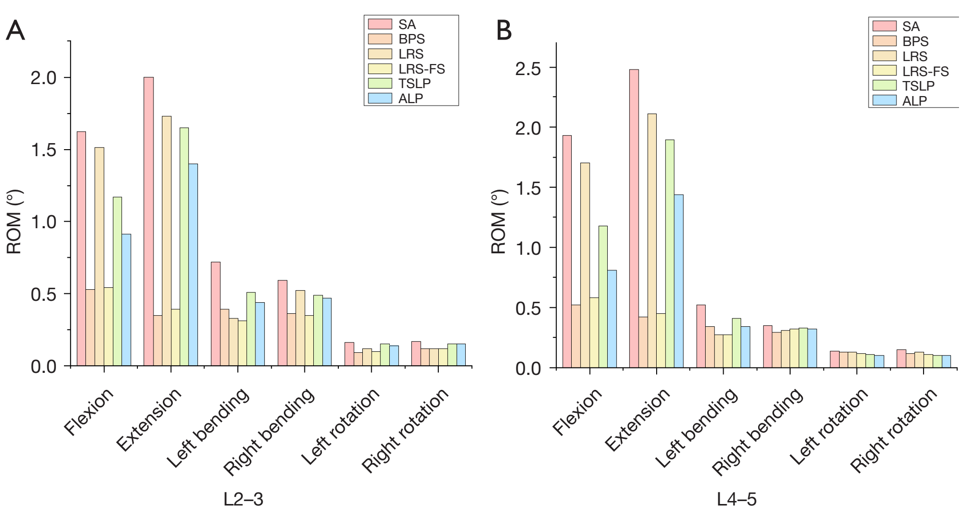

Figure 4 The range of motion of the L2–3 and L4–5 segments in models with various fixations. (A) The range of motion of the L2–3 segments in models with various fixations. (B) The range of motion of the L4–5 segments in models with various fixations. SA, stand-alone; BPS, bilateral pedicle screw; LRS, lateral rod-screw; LRSFS, lateral rod-screw plus facet screw; TSLP, two-screw lateral plate; ALP, anatomical lateral plate; ROM, range of motion.

flexion, the maximum stress of the cage was larger in the SA and LRS models, while the maximum stress in the BPS and ALP models was smaller. The maximum stress of the cage with the various supplementary internal fixations was smaller than the stress of the SA model in the left bending states. Except for the BPS model, all other supplementary

Table 4 The maximum Von-mises stress of the cage (MPa)

Model	Flexion	Extension	Left bending	Right bending	Left rotation	Right rotation
L2–3						
SA	36.78	28.48	28.37	20.38	21.12	18.88
BPS	23.61	17.62	25.01	24.23	17.45	19.99
LRS	35.31	21.89	14.47	17.95	14.55	14.95
LRSFS	25.62	7.37	14.36	19.12	16.02	16.09
TSLP	26.61	31.79	18.81	19.68	16.78	13.34
ALP	23.04	24.95	14.81	18.28	13.61	10.48
L4–5						
SA	53.77	36.26	55.15	25.95	32.75	23.26
BPS	37.27	13.28	41.53	20.45	28.56	20.35
LRS	40.71	28.33	26.74	22.22	18.11	15.06
LRSFS	23.96	13.42	25.69	22.02	19.80	14.62
TSLP	23.77	31.00	19.90	25.04	11.71	12.74
ALP	16.42	25.15	15.53	21.64	11.31	9.67

SA, stand-alone; BPS, bilateral pedicle screw; LRS, lateral rod-screw; LRSFS, lateral rod-screw plus facet screw; TSLP, two-screw lateral plate; ALP, anatomical lateral plate.

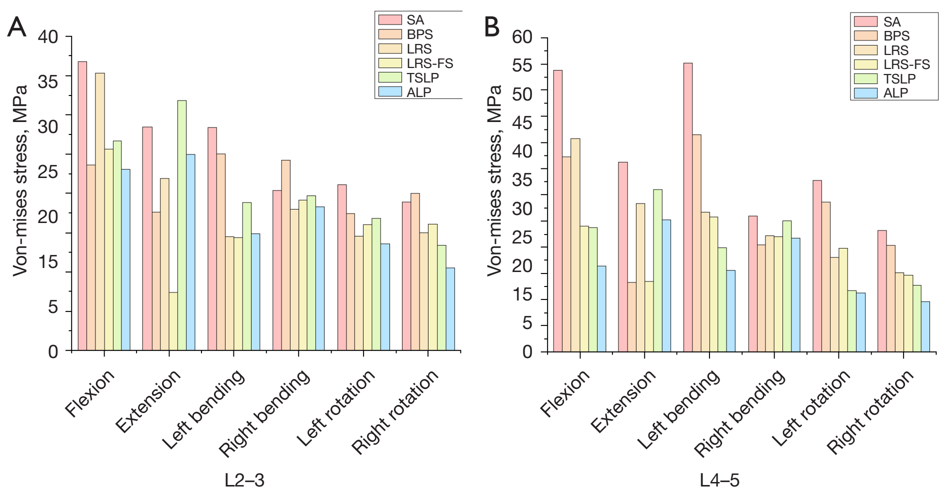

Figure 5 The maximum Von-mises stress of the cage. (A) The maximum von-mises stress of the cage in L2–3 models with various fixations. (B) The maximum von-mises stress of the cage in L4–5 model with various fixations. SA, stand-alone; BPS, bilateral pedicle screw; LRS, lateral rod-screw; LRSFS, lateral rod-screw plus facet screw; TSLP, two-screw lateral plate; ALP, anatomical lateral plate.

fixation models showed less maximum stress than the SA model in the right bending states. In both left and right rotation movements, the maximum stress of the cage of the ALP models was smallest among all models. It was noted that the anatomical plates showed better biomechanical performance concerning the cage stress in all motion states. Similar to the findings of ROMs, among the ALP models in different motion states, the maximum stress of the cages was the largest in flexion/extension were largest while the stress of the cages in lateral/right rotation were smallest.

Table 5 The maximum loading of the plates and screws (MPa)

Model	Flexion	Extension	Left bending	Right bending	Left rotation	Right rotation
L2–3						
BPS	128.17	128.54	64.67	46.48	50.19	60.48
LRS	78.09	91.58	49.28	15.05	29.74	29.26
LRSFS	54.56	67.64	47.00	47.30	35.99	29.54
TSLP	77.31	76.33	47.11	13.54	37.34	32.31
ALP	62.58	62.58	38.81	22.31	29.29	38.90
L4–5						
BPS	166.6	115.75	83.16	83.57	71.83	72.36
LRS	93.14	86.02	48.90	15.26	32.68	25.49
LRSFS	67.95	71.53	48.01	55.22	32.84	31.59
TSLP	79.81	80.62	57.88	25.60	39.38	33.99
ALP	112.27	108.39	89.75	45.94	51.64	54.83

BPS, bilateral pedicle screw; LRS, lateral rod-screw; LRSFS, lateral rod-screw plus facet screw; TSLP, two-screw lateral plate; ALP, anatomical lateral plate.

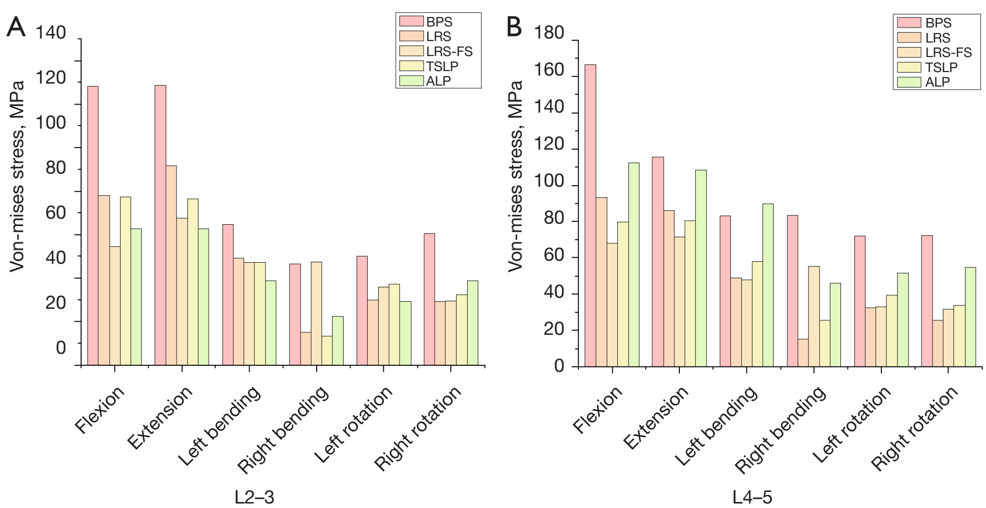

Figure 6 The maximum loading of the plates and screws. (A) The maximum loading of the plates and screws in L2–3 models with various fixations. (B) The maximum loading of the plates and screws in L4–5 model with various fixations. BPS, bilateral pedicle screw; LRS, lateral rod-screw; LRSFS, lateral rod-screw plus facet screw; TSLP, two-screw lateral plate; ALP, anatomical lateral plate.

The L4–5 model results are shown in *Table 4* and *Figure 5*. The maximum stress of the cage was smallest in the ALP model in the flexion, left bending, left rotation, and right rotation states. The anatomical plate was also biomechanically superior to the two-hole lateral plates. And the cage stress in in lateral/right rotation were smallest as well.

Stress of the internal fixation

The maximum stress of the internal fixations in the L2–3 and L4–5 models is presented in *Table 5* and *Figures 6,7*. In the L2–3 model, the stress of the internal fixation in the ALP model was less than the BPS model in all movement states and was close to the stress in the LRSFS model.

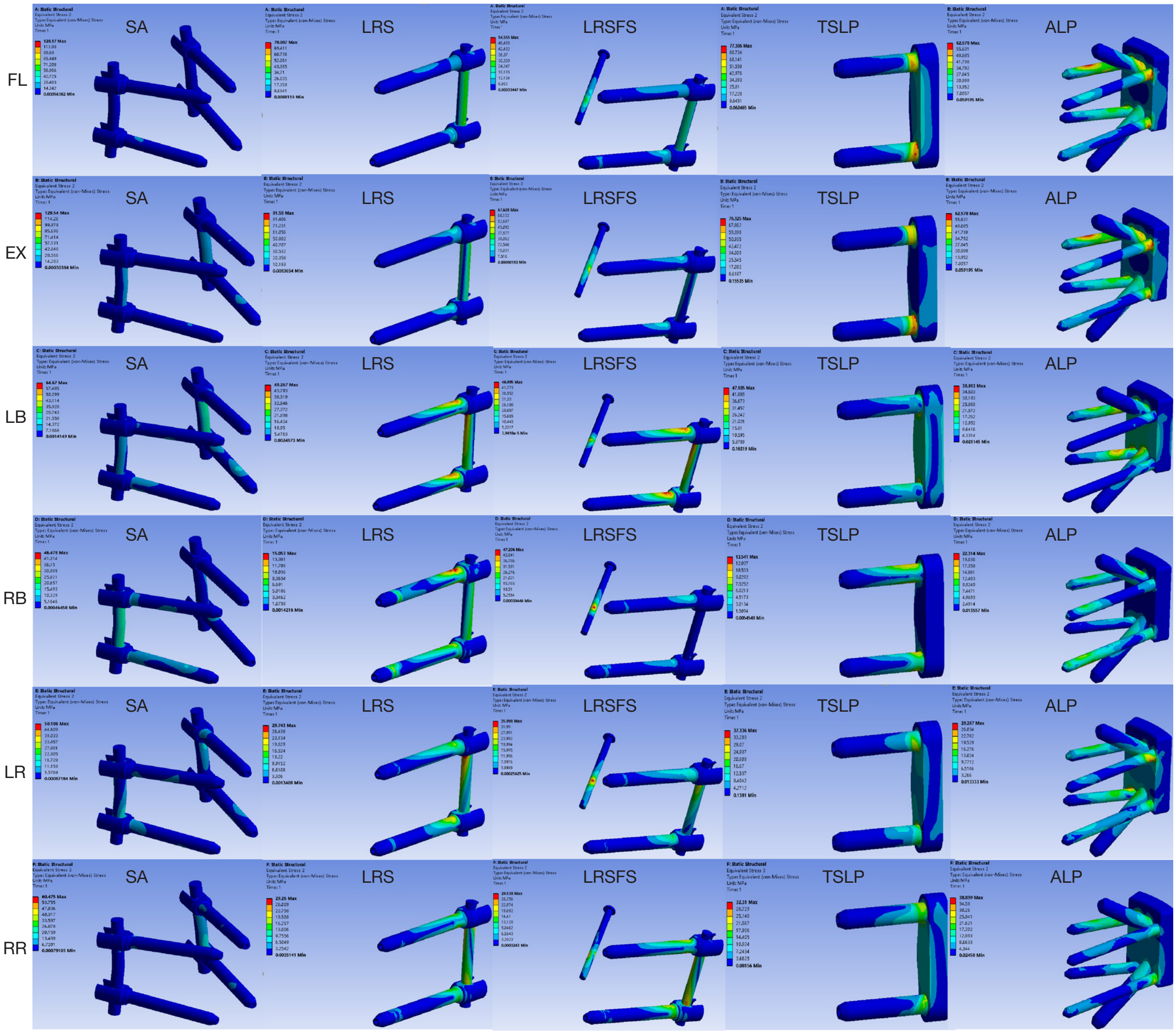

Figure 7 The stress distribution on various fixations under different motion states. SA, stand-alone; LRS, lateral rod-screw; LRSFS, lateral rod-screw plus facet screw; TSLP, two-screw lateral plate; ALP, anatomical lateral plate; FL, flexion; EX, extension; LB, lateral bending; RB, right bending; LR, left rotation; RR, right rotation.

Similarly, less maximum stress of the fixation was found in the ALP model compared with the BPS model in all motion states except for left bending. With regard to the stress of ALP models in different motion states, the stress was larger in flexion, extension and left bending movements than the other three movements.

Discussion

The prevention of postoperative complications, such as displacement and subsidence of the cage, plays a significant role in maintaining the surgical efficacy of OLIF. According to previous studies, the incidence of complications associated with the cage was about 2.9–13.4% (3,19). The specific causes of cage subsidence remain to be studied, but previous studies have suggested that osteoporosis, multi-level fusion, and endplate injury were potential risk factors (20,21). Among them, there may be a causal relationship between endplate injury and cage subsidence. The over-concentration of the stress on the endplate leads to endplate injury and vertebral trabecular bone injury, which could affect the supporting force towards the cage, causing cage subsidence. Conversely, cage subsidence would result in further stress concentration and thus forms a vicious circle (6). This study found that the SA fixation technique was associated with larger ROMs. The larger ROMs indicated that SA fixation was less stable than the cage models with supplementary fixation instruments, which could potentially reduce the rate of interbody fusion. Among different fixation instruments, BPS and LRSFS could provide three-column fixation so that their efficiency on restricting the movements was superior, particularly in extension and flexion movements. LRS and TSLP perform worst in reducing the ROMs because the two fixations mainly relying on the two screws installed into the vertebral body. The number and directions of the screw limited their capability of restricting the movements. This could explain why the ALP with more screws and different directions provide better stability than TSLP in all motion states. Given that the ALP mainly fixed the anterior and middle spinal column and the original range of motion in flexion/extension for human lumbar spine was the largest, ROMs of ALP models in flexion/extension motion states were the largest compared to ROMs of other motion states.

In terms of cage stress, the maximum stress of the SA cage was largest in the flexion, left bending, and left rotation states in the L2–3 segment. Additionally, the maximum stress of the SA cage was ranked second among the six models in other motion movements. In the L4–5 model, the maximum stress of the SA cage was the largest in all movement states. In the flexion and left bending states, the maximum stress of the cage was 53.77 and 55.15 MPa, respectively, which were close to the yield strength of the vertebral endplates (22). Therefore, the risk of cage subsidence would be high. Moreover, if patients have osteoporosis and previous endplate injury, the risk will be increased. By installing the plates or screws as supplementary fixation, the stress could be dispersed. Therefore, according to our results, supplementary fixation with internal fixation instruments will help to reduce the risk of complications for patients with osteoporosis and endplate injury. This finding is also consistent with previous studies (14,23). As *Figures 6,7* shows, BPS performs best in restricting the movements but the fixation would have the largest stress. However, the LRSFS and ALP could provide satisfactory stability with acceptable maximum stress of internal fixation system. This superiority was also associated with the number, direction and position of the screws, which would affect the loading of the cage or the internal fixations. This could be reflected by the finding that the stress of ALP models was larger in flexion, extension and left bending movements than the other three movements.

One of the most significant strengths of the current study is the anatomical design of the plates. To further study the fixation stability and stiffness and to realize the translational value of the design, future researches based on cadaveric specimen models were needed, which was a series of costly and time-consuming procedures. The findings in the study preliminarily provided the theoretical basis and could help save the cost and time during the cadaveric test.

BPS has been considered as the gold standard fixation because of its rigid structure due to the three-column fixation. And LRSFS also showed good biomechanical efficiency in this study. But the installation of BPS and LRSFS requires extra incision, radiation exposure and intraoperative position change. And the risk of injury on in surrounding structures, such as paraspinal muscles, nerve root and vessels, increased in the procedure (5). Previous literature has reported that using lateral plates could minimize the operative time and blood loss, which allows surgeons achieve decompression and fusion through a single incision and position (24). Compared with conventional two-screw lateral plates, the anatomical plates were designed based on our anatomical researches, which could provide both short-term and long-term benefits. At present, a major concern of using lateral plates is that the segmental arteries might be injured during the installation, and the injury could affect clinical efficacy and even be life-threatening (2,25). Thus, the plate length should be limited according to the vascular intervals between the segmental arteries. Our previous study used computed tomography angiography and acquired precise and comprehensive parameters of the segmental arteries (11). We found that the L5 segmental artery was absent in most people, and thus the length of the plates used for L4–5 OLIF could be designed more flexibly. To avoid injury to the aorta and lumbar plexus, the width was based on the data measured by ourselves of the theoretical surgical corridor (see Figure S1 and Table S1). Thus, it would help decrease the risk of intra-operative vascular injury. The sagittal curvature refers to the lumbar lordosis angle provided by previously published data (18). The curvatures of the anterior lateral border of the endplates were found to stay constant at 0.60 cm^{-1} at all lumbar segments in our previous study (12). The curvature of the plates was determined accordingly to fully fit the anterior side of the vertebral body. The curvature match between the plates and vertebrae could decrease the risk of construct failure caused by an extended bending moment and excessive intraoperative bending (26,27). As for the screw design, the plates adopted a strategy combining cancellous bone screws and cortex bone screws. The central two screws were cancellous bone screws towards the center of the vertebral body. The screws made full use of the height of the vertebral body and maintained safety while increasing the length of the screw. At the same time, four surrounding cortical bone screws reached the contralateral endplate cortex to increase the fixation strength as well as to restrict the segmental movements, which could increase the instant segmental surgery after the surgery. Meanwhile, the screws inserted into the vertebral endplates sustained the endplates and thus decreased the risk of subsidence in the long term. In addition, the two cortical bone screws on the same side along the discs stayed at a specific angle to enhance pullout resistance to avoid the construct failure.

Previous biomechanical tests have mainly focused on a single segment, but in this case, the simulation results might not be solid enough for the other uninvolved segments in the study (5,7). Thus, the current study chose both L2–3 and L4–5 segments for modeling, and the results confirmed the efficacy of this design. Moreover, previous studies have mostly applied only one plate of a specific size for simulation, but it should be noted that during the OLIF surgical procedure, a one-size plate might not fit all segments. The current study designed two sizes for different segments based on our anatomical studies, thus offering translational value. The anatomical design and verification at both upper and lower lumbar segments are two important advantages of our method, which was distinguished from previous studies. With the anatomical design described above, the plates could theoretically provide better biomechanical stability than conventional lateral endplates.

Compared with the SA and conventional two-screws plate techniques for OLIF, the current study found that anatomical plates reduced the cage stress as well as the mobility of the segment, indicating that the plates were capable of reducing the risk of cage subsidence and pseudoarthrosis. Additionally, the maximum stress of the anatomical plates was smaller than that of the BPSs, which means that the construct failure risk was not significantly higher for the anatomical plates. It should be noted that the anatomical plates can be implanted through one single incision and one single procedure without the need to reposition under anesthesia. Furthermore, using anatomical plates could help protect posterior structures, such as the paravertebral muscles. The reduction in blood loss, shorter surgical time, and less radiation exposure correspond to the concept of 'enhanced recovery after surgery'.

There are a few limitations to this study. First, as previous studies have admitted, the finite element analysis has its own intrinsic disadvantage. Although finite element analysis is a satisfactory non-invasive method with simplicity and accuracy which allows building complex models and calculating relevant biomechanical properties, some acceptable idealized simulations were applied during the procedures (28,29). In another word, the model was simplified, whereas the actual boundary and loading conditions would be more complicated. Furthermore, the CT images were acquired from a subject without severe degenerative disease to simulate the postoperative situations, thus the results might not be generalizable to patients with severe bony degeneration. However, as patients with severe bony degeneration are not ordinarily indicated for OLIF surgery, the bias might be acceptable.

Conclusions

The current study established an initial design of novel anatomical plates for OLIF surgery based on the anatomical parameters obtained in our previous research. Moreover, the current research verified the biomechanical efficacy of the plates through finite element study at the L2–3 and L4–5 lumbar spine segments. In the L2–3 and L4–5 segment models, the anatomical plates reduced the maximum stress of the cage under each motion state, thus reducing the cage subsidence risk. Furthermore, the anatomical plates could effectively limit the ROMs and increase the stability of internal fixations under various motion states. The self-designed anatomical plates also performed better than the two-screw plates. The anatomical plates should be considered as supplementary fixations using a single incision and position to improve the efficacy of OLIF and reduce the risk of complications.

Acknowledgments

Funding: This work was supported by grants from the No. 2021-NCRC-CXJJ-ZH-18 of Clinical Application-oriented Medical Innovation Foundation from National Clinical Research Center for Orthopedics, Sports Medicine & Rehabilitation and Jiangsu China—Israel Industrial Technical Research Institute Foundation, the Support Project of Biomedical Technology of Shanghai Science and

Technology Innovation Action Plan (No. 19441902200), and the Excellent Talent Training Award Program of Huashan Hospital, Fudan University.

Footnote

Reporting Checklist: The authors have completed the MDAR reporting checklist. Available at https://atm.amegroups.com/article/view/10.21037/atm-22-3456/rc

Data Sharing Statement: Available at https://atm.amegroups.com/article/view/10.21037/atm-22-3456/dss

Conflicts of Interest: All authors have completed the ICMJE uniform disclosure form (available at https://atm.amegroups.com/article/view/10.21037/atm-22-3456/coif). All authors report that the design of the anatomical plates used in the study has received a utility model patent in China (No. ZL202121374755.X). HW reports that this work was supported by grants from the No. 2021-NCRC-CXJJ-ZH-18 of Clinical Application-oriented Medical Innovation Foundation from National Clinical Research Center for Orthopedics, Sports Medicine & Rehabilitation and Jiangsu China—Israel Industrial Technical Research Institute Foundation, the Support Project of Biomedical Technology of Shanghai Science and Technology Innovation Action Plan (No. 19441902200) and the Excellent Talent Training Award Program of Huashan Hospital, Fudan University. The authors have no other conflicts of interest to declare.

Ethical Statement: The authors are accountable for all aspects of the work in ensuring that questions related to the accuracy or integrity of any part of the work are appropriately investigated and resolved. All participating patients signed informed consent to participate in this study, and any information or identification of the patients have been concealed. The study was conducted in accordance with the Declaration of Helsinki (as revised in 2013). This study was approved by the institutional review board of Huashan Hospital, Fudan University (No. KY-2020-052).

References

1. Hah R, Kang HP. Lateral and Oblique Lumbar Interbody Fusion-Current Concepts and a Review of Recent Literature. Curr Rev Musculoskelet Med 2019;12:305-10.
2. Silvestre C, Mac-Thiong JM, Hilmi R, et al. Complications and Morbidities of Mini-open Anterior Retroperitoneal Lumbar Interbody Fusion: Oblique Lumbar Interbody Fusion in 179 Patients. Asian Spine J 2012;6:89-97.
3. Woods KR, Billys JB, Hynes RA. Technical description of oblique lateral interbody fusion at L1-L5 (OLIF25) and at L5-S1 (OLIF51) and evaluation of complication and fusion rates. Spine J 2017;17:545-53.
4. Wu H, Cheung JPY, Zhang T, et al. The Role of Hounsfield Unit in Intraoperative Endplate Violation and Delayed Cage Subsidence with Oblique Lateral Interbody Fusion. Global Spine J 2021. [Epub ahead of print]. doi: 10.1177/21925682211052515.
5. Guo HZ, Tang YC, Guo DQ, et al. Stability Evaluation of Oblique Lumbar Interbody Fusion Constructs with Various Fixation Options: A Finite Element Analysis Based on Three-Dimensional Scanning Models. World Neurosurg 2020;138:e530-8.
6. He W, He D, Sun Y, et al. Standalone oblique lateral interbody fusion vs. combined with percutaneous pedicle screw in spondylolisthesis. BMC Musculoskelet Disord 2020;21:184.
7. Wang Y, Wang J, Tu S, et al. Biomechanical Evaluation of an Oblique Lateral Locking Plate System for Oblique Lumbar Interbody Fusion: A Finite Element Analysis. World Neurosurg 2022;160:e126-41.
8. Cai Z, Ma R, Zhang J, et al. Evaluation of the Stability of a Novel Lateral Plate Internal Fixation: An In Vitro Biomechanical Study. World Neurosurg 2021. [Epub ahead of print]. doi: 10.1016/j.wneu.2021.10.164.
9. Fujibayashi S, Kawakami N, Asazuma T, et al. Complications Associated With Lateral Interbody Fusion: Nationwide Survey of 2998 Cases During the First 2 Years of Its Use in Japan. Spine (Phila Pa 1976) 2017;42:1478-84.
10. Abe K, Orita S, Mannoji C, et al. Perioperative Complications in 155 Patients Who Underwent Oblique Lateral Interbody Fusion Surgery: Perspectives and

Indications From a Retrospective, Multicenter Survey. Spine (Phila Pa 1976) 2017;42:55-62.
11. Huang W, Zhou P, Xie L, et al. The trajectory characteristics and clinical significance of the left-sided lumbar segmental artery: a prospective cross-sectional radio-anatomical study. Quant Imaging Med Surg 2022;12:1977-87.
12. Huang W, Wang H, Zhou P, et al. Analysis of the Curvature and Morphologic Features of the Lumbar Vertebral Endplates Through the Transverse Section: A Radioanatomical Study. World Neurosurg 2021;150:e500-10.
13. Goel VK, Kong W, Han JS, et al. A combined finite element and optimization investigation of lumbar spine mechanics with and without muscles. Spine (Phila Pa 1976) 1993;18:1531-41.
14. Lu T, Lu Y. Comparison of Biomechanical Performance Among Posterolateral Fusion and Transforaminal, Extreme, and Oblique Lumbar Interbody Fusion: A Finite Element Analysis. World Neurosurg 2019;129:e890-9.
15. Iyer S, Christiansen BA, Roberts BJ, et al. A biomechanical model for estimating loads on thoracic and lumbar vertebrae. Clin Biomech (Bristol, Avon) 2010;25:853-8.
16. Zhao L, Chen J, Liu J, et al. Biomechanical analysis on of anterior transpedicular screw-fixation after two-level cervical corpectomy using finite element method. Clin Biomech (Bristol, Avon) 2018;60:76-82.
17. Yamamoto I, Panjabi MM, Crisco T, et al. Three-dimensional movements of the whole lumbar spine and lumbosacral joint. Spine (Phila Pa 1976) 1989;14:1256-60.
18. Barrey C, Darnis A. Current strategies for the restoration of adequate lordosis during lumbar fusion. World J Orthop 2015;6:117-26.
19. Ohtori S, Mannoji C, Orita S, et al. Mini-Open Anterior Retroperitoneal Lumbar Interbody Fusion: Oblique Lateral Interbody Fusion for Degenerated Lumbar Spinal Kyphoscoliosis. Asian Spine J 2015;9:565-72.
20. Ge T, Ao J, Li G, et al. Additional lateral plate fixation has no effect to prevent cage subsidence in oblique lumbar interbody fusion. J Orthop Surg Res 2021;16:584.
21. Kotheeranurak V, Jitpakdee K, Lin GX, et al. Subsidence of Interbody Cage Following Oblique Lateral Interbody Fusion: An Analysis and Potential Risk Factors. Global Spine J 2021. [Epub ahead of print]. doi: 10.1177/21925682211067210.
22. Frost HM. A 2003 update of bone physiology and Wolff's Law for clinicians. Angle Orthod 2004;74:3-15.
23. Zhao WT, Qin DP, Zhang XG, et al. Biomechanical effects of different vertebral heights after augmentation of osteoporotic vertebral compression fracture: a three-dimensional finite element analysis. J Orthop Surg Res 2018;13:32.
24. Li HD, Zhong L, Min JK, et al. Oblique lateral interbody fusion combined with lateral plate fixation for the treatment of degenerative diseases of the lumbar spine: A retrospective study. Medicine (Baltimore) 2022;101:e28784.
25. Ntourantonis D, Tsekouras V, Korovessis P. Delayed Fatal Lumbar Artery Bleeding Following Less Invasive Posterolateral Decompression and Fusion. Spine (Phila Pa 1976) 2018;43:E976-9.
26. Schmutz B, Wullschleger ME, Kim H, et al. Fit assessment of anatomic plates for the distal medial tibia. J Orthop Trauma 2008;22:258-63.
27. Petersik A, Homeier A, Hoare SG, et al. A numeric approach for anatomic plate design. Injury 2018;49 Suppl 1:S96-S101.
28. Li Y, Fogel GR, Liao Z, et al. Prosthesis and Hybrid Strategy Consideration for Treating Two-level Cervical Disc Degeneration in Hybrid Surgery. Spine (Phila Pa 1976) 2018;43:379-87.
29. Wu TK, Meng Y, Liu H, et al. Biomechanical effects on the intermediate segment of noncontiguous hybrid surgery with cervical disc arthroplasty and anterior cervical discectomy and fusion: a finite element analysis. Spine J 2019;19:1254-63.

(English Language Editor: D. Fitzgerald)

Cite this article as: Huang W, Tian Y, Ma X, Lv F, Wang H, Jiang J. Biomechanical evaluation of a novel anatomical plate for oblique lumbar interbody fusion compared with various fixations: a finite element analysis. Ann Transl Med 2022;10(16):871. doi: 10.21037/atm-22-3456

Supplementary

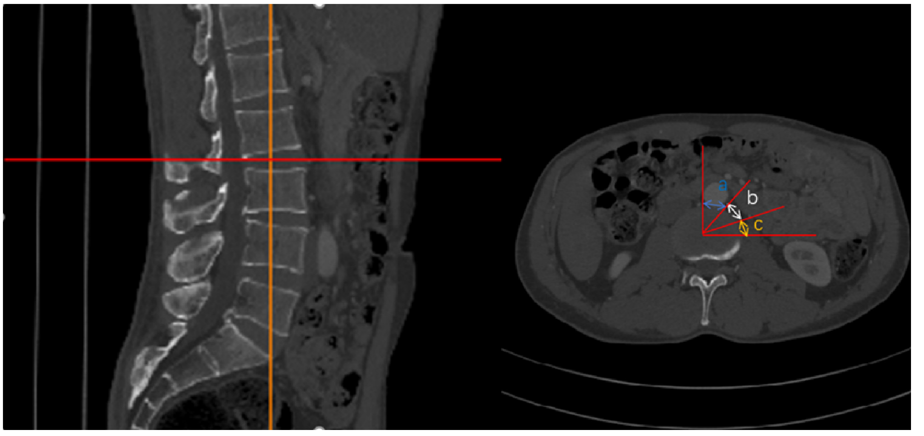

Figure S1 The measurement of the surgical corridor. The region 'a' refers to the edge of the vertebrae covered by the abdominal aorta (aorta corridor). The region 'b' refers to the edge without any covered structure (exposed corridor) while the letter 'c' refers to the region covered by the psoas of the anterior-lateral vertebral (psoas corridor).

Table S1 The values of the surgical corridor

Corridor	Aorta corridor	Exposed corridor	Psoas corridor	Ideal corridor*
L1-2				
Maximum value	15.7	23.2	12.8	30.2
Minimum value	7.8	7.7	2	15.6
Mean ± SD	12.1±1.5	13.3±3.8	7.5±2.7	20.8±3.5
Mean-2*SD	9.1	5.6	2.2	13.9
L2-3				
Maximum value	14.7	19.3	20	32.3
Minimum value	8.8	6.4	5.5	14.9
Mean ± SD	11.2±1.2	13.0±3.1	10.9±3.0	23.8±3.8
Mean-2*SD	8.8	6.8	5	16.3
L3-4				
Maximum value	15.3	22.5	21	34.8
Minimum value	8.1	6.2	6.0	15.3
Mean ± SD	11.3±1.5	13.1±3.8	12.9±3.7	26.0±4.3
Mean-2*SD	8.4	5.5	5.6	17.4
L4-5				
Maximum value	23.4	22.1	19.9	33.4
Minimum value	6.6	1.3	5.8	10.6
Mean ± SD	10.6±3.6	9.4±3.6	13.8±3.8	23.2±5.5
Mean-2*SD	3.4	2.2	6.2	12.1

*, Ideal corridor = Exposed corridor + Psoas corridor.

 https://dx.doi.org/10.21037/atm-22-3456